

Colorectal Image Classification Using Randomized Neural Network Descriptors

Jarbas Joaci de Mesquita Sá Junior¹ ^a and André Ricardo Backes² ^b

¹*Programa de Pós-Graduação em Engenharia Elétrica e de Computação, Brazil*

²*Department of Computing, Federal University of São Carlos, Brazil*

Keywords: Randomized Neural Network, Colorectal Database, Texture Analysis.

Abstract: Colorectal cancer is among the highest incident cancers in the world. A fundamental procedure to diagnose it is the analysis of histological images acquired from a biopsy. Because of this, computer vision approaches have been proposed to help human specialists in such a task. In order to contribute to this field of research, this paper presents a novel way of analyzing colorectal images by using a very discriminative texture signature based on weights of a randomized neural network. For this, we addressed an important multi-class problem composed of eight types of tissues. The results were promising, surpassing the accuracies of many methods present in the literature. Thus, this performance confirms that the randomized neural network signature is an efficient tool for discriminating histological images from colorectal tissues.

1 INTRODUCTION

Colorectal cancer (CRC) remains among the most prevalent types of cancer in the global population. It is considered the third prevalent cancer type for estimated new diagnoses and deaths in United States in 2023 (Siegel et al., 2023). There are several tests to detect this disease (sigmoidoscopy, colonoscopy, high-sensitive fecal occult blood test etc.). However, it is fundamental to analyze histological images acquired from a biopsy to diagnose CRC (Yoon et al., 2019). These images reveal the complex structure of the tumor, which is composed of several different tissues, such as clonal tumor cells, stroma cells, necrotic areas, among others (Kather et al., 2016).


Traditionally, these images are evaluated by human specialists. Over the years, computer vision approaches have been proposed to analyze histological colorectal images in order to help the humans specialists with an extra opinion. Moreover, these computational methods have as an advantage to speed up the diagnosis process and to measure attributes not detected by the human eye. To cite recent instances, the paper (Peyret et al., 2018) applies a multispectral multiscale local binary pattern texture method to extract signatures from colorectal biopsy images. In


(Ribeiro et al., 2019), authors use fractal dimension, curvelet transforms, and co-occurrences matrices to extract features from two colorectal image datasets. The paper (dos Santos et al., 2018) combines sample entropy, multiscale approaches and a fuzzy strategy to classify histological colorectal images into benign and malign groups.

This work aims to classify the histological colorectal database publicly released by the paper (Kather et al., 2016) using a very discriminative texture analysis method based on randomized neural networks. To explain our work, this paper is organized as follows: Section 2 briefly describes how to construct a randomized neural network, and Section 3 explains how to adapt this network to build a texture analysis method. Section 4 shows the details of the database used and describes the classification procedure. Section 5 shows the obtained results and discusses them in the light of the accuracies obtained by compared methods. Finally, Section 6 presents some remarks about this work.

2 RANDOMIZED NEURAL NETWORK

Randomized neural networks (RNN) (Schmidt et al., 1992; Pao and Takefuji, 1992; Pao et al., 1994; Huang

^a  <https://orcid.org/0000-0003-3749-2590>

^b  <https://orcid.org/0000-0002-7486-4253>

et al., 2006), in their simplest architecture, are neural networks composed of a single hidden layer, whose weights are determined randomly according to a determined probability distribution. These weights enable the hidden layer to project the input feature vectors into another dimensional space aiming to separate them more easily, according to Cover's theorem (Cover, 1965). The output weights, in turn, can be determined using a closed-form solution whose inputs are the feature vectors projected by the hidden layer and the output label vectors.

To provide a brief mathematical explanation describing a simple variant of a randomized neural network with bias in the output layer, let $X = [\vec{x}_1, \vec{x}_2, \dots, \vec{x}_N]$ be a matrix composed of N input feature vectors, each one having p attributes. After including -1 as the first feature of each \vec{x}_i (for bias), the output of the hidden layer for all the input features in X can be obtained by computing $\phi(WQ)$, where $\phi(\cdot)$ is a transfer function and W is a matrix of weights whose dimensions are $Q \times (p+1)$. Let $Z = [\vec{z}_1, \vec{z}_2, \dots, \vec{z}_N]$ be a matrix of the feature vectors produced by the hidden layer, each one having Q attributes. As a final step, this matrix Z , after the inclusion of -1 as the first feature for each \vec{z}_i (for bias), can be used to build the matrix of weights of the output neuron layer, as follows

$$M = DZ^T (ZZ^T + \lambda I)^{-1}, \quad (1)$$

where $D = [\vec{d}_1, \vec{d}_2, \dots, \vec{d}_N]$ is a matrix of label vectors, $Z^T (ZZ^T)^{-1}$ is the Moore-Penrose pseudo-inverse (Moore, 1920; Penrose, 1955), and λI is the term for Tikhonov regularization (Tikhonov, 1963; Calvetti et al., 2000) (I is the identity matrix and λ is a regularization parameter).

3 IMPROVED RANDOMIZED NEURAL NETWORK SIGNATURE

An improved version of the randomized neural signature (Sá Junior and Backes, 2016) is presented in (Sá Junior and Backes,) and used in this work. This version proposes three different signatures as well as their combinations. In the first signature $\vec{\alpha}(Q)$, for a determined neighborhood in a window $K \times K$, each neighboring pixel is used as a label to fill a line vector D and the remainder as an input vector to fill an input matrix X . In the second signature $\vec{\beta}(Q)$, the X obtained in $\vec{\alpha}(Q)$ for each $K \times K$ window is also used as labels ($X = D$). In this case, it is necessary to com-

pute the mean of the weights because there is more than one neuron in the output layer. The third signature $\vec{\gamma}(Q)$ is similar to $\vec{\alpha}(Q)$, but the matrix X and D are exclusive for each window $K \times K$. Thus, we obtain the signature $\vec{\gamma}(Q)$ by computing the mean of the weights of all windows $K \times K$. The signatures $\vec{\alpha}(Q)$, $\vec{\beta}(Q)$ and $\vec{\gamma}(Q)$ are built by using $K = \{3, 5, 7\}$. In this work, we use the signature $\vec{\Omega}(Q)$, which is $\vec{\Omega}(Q) = [\vec{\alpha}(Q), \vec{\beta}(Q), \vec{\gamma}(Q)]$. More details on these signatures can be found in (Sá Junior and Backes,).

4 EXPERIMENTS

4.1 Colorectal Database

The colorectal database used in our experiments is presented in the paper (Kather et al., 2016) and available at DOI:10.5281/zenodo.53169. It contains 5,000 images divided into 8 classes (625 images per class). The classes are: Tumor epithelium; Simple stroma; Complex stroma; Immune cells; Debris; Normal mucosal glands; Adipose tissue; and Background. Figure 1 shows one sample for each class.

4.2 Experimental Setup

To classify the texture signatures, we applied a Radial-Basis SVM (Boser et al., 1992; Cortes and Vapnik, 1995) with $C = 20$ by using LIBSVM (Chang and Lin, 2011). The validation strategy adopted was 5-fold, that is, the signature database is even divided into five groups, one group used for testing and the remainder for training. Thus procedure is repeated five times (each time with a different group for testing). The mean accuracy is the performance measure. We computed three signatures $\vec{\Omega}(39)$, $\vec{\Omega}(39, 49, 59)$ and FUSRNN (Fusion of RNN signatures with other texture analysis methods) in the colorectal images converted into grayscale. The texture signatures concatenated in FUSRNN were:

- Complex Network Texture Descriptor (CNTD) (Backes et al., 2013): Complex Network Theory is employed to represent the pixels of a grayscale image as a dynamic complex network. Topological features of the network are then calculated to create a feature vector that characterizes the original image. The parameters utilized include a network modeling radius of $r = 3$ and 36 threshold values for generating dynamic transformations, i.e., how connections between vertices change. A total of 108 descriptors, comprising energy, en-

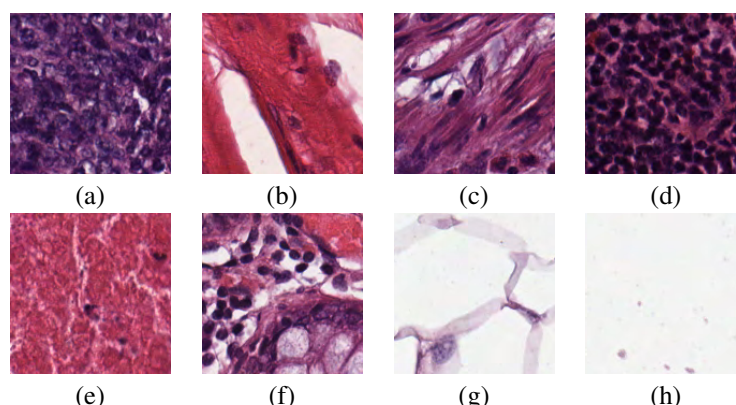


Figure 1: The colorectal database: (a) Tumor epithelium, (b) Simple stroma, (c) Complex stroma, (d) Immune cells, (e) Debris, (f) Normal mucosal glands, (g) Adipose tissue, (h) Background (Source: paper (Kather et al., 2016) and DOI:10.5281/zenodo.53169).

trophy, and contrast measurements from each transformation, were computed.

- Fourier descriptors (Weszka et al., 1976): In this approach, the input image undergoes the bi-dimensional Fourier transform, and subsequently, the shifting operator is applied to compute spectrum descriptors. The descriptor is obtained by summing the absolute coefficients located at the same radial distance from the image's center. By following this process, a total of 74 descriptors are generated.
- Gabor Filter (Daugman and Downing, 1995): A set of filters was generated using the mathematical procedure and the parameter values described in (Manjunath and Ma, 1996), that is, scales $S = 4$, rotations $K = 6$, and upper and lower frequencies $U_h = 0.4$ and $U_l = 0.05$, respectively. Next, mean and standard-deviation were computed from these filters, thus resulting in 48 features.
- Gray Level Dependence Matrix (GLDM) (Weszka et al., 1976): In this method, the probability-density function is calculated for pairs of pixels with a given distance and intersample space, representing a specific absolute difference in intensity. For the experiments, four distances $((0, d), (-d, d), (d, 0), \text{ and } (-d, -d))$ and three intersample spaces $(d = 1, 2, 5)$ were used. From each probability-density function, five measurements (angular second moment, entropy, contrast, mean, and inverse difference moment) were computed. This process yields a total of 60 descriptors.
- Local Binary Patterns (LBP) (Ojala et al., 2002): this texture descriptor characterizes the local structure of an image by comparing the values of a central pixel with the intensities of its neighboring

pixels. LBP encodes this comparison result into a binary pattern, where each bit represents whether the neighboring pixel is greater or smaller in intensity compared to the central pixel. This enables LBP to capture texture information, such as edges, corners, and texture regularity. For the experiments, we used the LBP histogram computed using $(P, R) = (8, 1)$, resulting in 10 descriptors.

- Joint Adaptive Median Binary Patterns (Hafiane et al., 2015): This approach employs a combination of Local Binary Pattern (LBP) and Median Binary Pattern (MBP) techniques, enhanced by adaptive threshold selection, to extract local patterns from an image. As a result, a feature vector consisting of 320 descriptors is obtained, effectively representing the intricate local microstructure of the texture.

5 RESULTS AND DISCUSSION

In Table 1, we compared the accuracies of signatures $\vec{\Omega}(39)$, $\vec{\Omega}(39, 49, 59)$ and FUSRNN with the results showed in the paper (Wang et al., 2017). The comparison demonstrates that the descriptor in $\vec{\Omega}(39)$ surpasses almost all compared approaches. In turn, the accuracy of the signature $\vec{\Omega}(39, 49, 59)$ ($92.46\% \pm 0.44\%$) presents a result equivalent to the best performance in (Wang et al., 2017) ($92.6\% \pm 1.2\%$) and the result of FUSRNN surpasses all the compared approaches in Table 1.

We also compared the randomized network descriptors as well as their fusion with other texture analysis methods with the results in (Nanni et al., 2019). The result of $\vec{\Omega}(39)$, which was the signature used in (Sá Junior and Backes,) for compari-

Table 1: Comparison of performance of the randomized neural networks descriptors ($\vec{\Omega}(39)$ and $\vec{\Omega}(39, 49, 59)$) and its fusion with other methods (**FUSRNN**) with other approaches. The compared results were obtained from (Wang et al., 2017).

Approaches and accuracies (%)				
Histogram-lower 80.8	Histogram-higher 72.4	LBP 76.2	GLCM 71.9	Gabor 63.1
Perception 62.9	Best2 85.8	Best3 86.0	Best4 86.5	Best5 87.4
All-6 87.4	CNN 90.2 ± 3.1	CNN-H 89.2 ± 1.1	CNN-E 86.1 ± 1.4	BCNN 92.6 ± 1.2
$\vec{\Omega}(39)$ 91.34 ± 0.81	$\vec{\Omega}(39, 49, 59)$ 92.46 ± 0.44	FUSRNN 94.36 ± 0.30	-	-

Table 2: Comparison of performance of the randomized neural networks descriptors ($\vec{\Omega}(39)$ and $\vec{\Omega}(39, 49, 59)$) and its fusion with other methods (**FUSRNN**) with other approaches. The compared results were obtained from (Nanni et al., 2019).

Approaches and accuracies (%)			
LTP 87.6	MLPQ 92.48	CLBP 90.38	RICLBP 87.88
GOLD 84.46	HOG 65.60	AHP 92.28	FBSIF 92.30
FUS_1 92.24	FUS_2 93.26	FUS_3 93.54	FUS_4 93.74
CLM_1 87.70	CLM_2 86.52	CLM_3 78.02	CLM_4 86.32
CLM 85.08	CLoVo_1 87.26	CLoVo_2 62.72	CLoVo_3 86.80
CLoVo_4 89.26	CLoVo 89.08	FUS_CLM3 84.82	FUS_CLM 88.50
DeepOutput 91.90	DeepScores 94.44	FUS_ND(2) 92.72	FUS_ND(3) 93.02
FUS_D(0.5) 94.44	FUS_ND(3)+DeepOutput 93.24	FUS_ND(3)_FUS_D(0.5) 93.98	$\vec{\Omega}(39)$ 91.34 ± 0.81
$\vec{\Omega}(39, 49, 59)$ 92.46 ± 0.44	FUSRNN 94.36 ± 0.30	-	-

Table 3: Comparison of performance of the randomized neural networks descriptors ($\vec{\Omega}(39)$ and $\vec{\Omega}(39, 49, 59)$) and its fusion with other methods (**FUSRNN**) with other approaches. The compared results were obtained from (Paladini et al., 2021).

Approaches and accuracies (%)		
LPQ, SVM 68.12	BSIF, SVM 68.10	LPQ+BSIF, SVM 74.10
LPQ, NN 69.02	BSIF, NN 71.04	LPQ+BSIF, NN 74.22
ResNet-101 95.92	ResNeXt-50 95.74	Inception-v3 93.98
DenseNet-161 95.60	Mean-Ensemble-CNNs 96.16	NN-Ensemble-CNNs 96.14
$\vec{\Omega}(39)$ 91.34 ± 0.81	$\vec{\Omega}(39, 49, 59)$ 92.46 ± 0.44	FUSRNN 94.36 ± 0.30

son with other approaches, surpasses the performance of several compared methods in Table 2. The result of $\vec{\Omega}(39, 49, 59)$, in turn, is only surpassed by more sophisticated approaches based on ensembles (for instance, FUS_2) or Convolutional Neural Net-

works (for instance, DeepScores). On the other hand, our proposed signature FUSRNN provided a result (94.36% ± 0.30%) virtually equivalent to the best performance in Table 2 (DeepScores, with 94.44%).

In Table 3, we performed a comparison with the

results showed in (Paladini et al., 2021). This table shows that the three signatures $\tilde{\Omega}(39)$, $\tilde{\Omega}(39, 49, 59)$ and FUSRNN largely outperformed all the hand-crafted methods. On the other hand, almost all CNN-based approaches surpassed FUSRNN (exception for Inception-v3), with NN-Ensemble-CNNs presenting an advantage of 1.78%. To explain this difference in performance, it is important to stress that the authors in (Paladini et al., 2021) affirm that ResNet-101, ResNeXt-50, Inception-v3, and DenseNet-161 are “four of the most powerful CNN architectures”(Paladini et al., 2021) and that they used pre-trained models from the ImageNet Challenge Database. Moreover, the best CNN-based approach (NN-Ensemble-CNNs) is an ensemble combining the four mentioned CNN architectures.

Finally, the signature $\tilde{\Omega}(39, 49, 59)$ provides an accuracy equivalent to ARA-CNN (Raczkowski et al., 2019) ($92.24 \pm 0.82\%$), and the signature FUSRNN overcomes it. Thus, based on our results, it is possible to affirm that randomized neural network descriptors ($\tilde{\Omega}(39)$ and $\tilde{\Omega}(39, 49, 59)$) have high performance, surpassing several texture analysis methods. Also, when associated with other descriptors (FUSRNN), it provided accuracies slightly inferior to the best CNN architectures. Such performance suggests that novel improvements in the RNN signature as well as its association with other descriptors equally discriminative may result in even higher accuracies when applied to colorectal images.

6 CONCLUSION

This paper presented an application of a highly discriminative texture descriptor based on weights of randomized neural network on a very important multi-class problem, which consists of discriminating colorectal images into eight classes, according to the image database provided by (Kather et al., 2016). The results of the randomized neural network signature were promising, surpassing several texture analysis methods. When the neural neural descriptors were associated with other texture analysis methods, this fusion signature was capable of providing accuracies similar or slightly inferior to that of several powerful convolutional neural networks, which are known for having a high number of parameters to tune. Thus, ground on our results, we believe that our proposed applied approach has potential to provide even better results and adds a valuable tool to the computer vision research in colorectal images.

ACKNOWLEDGEMENTS

This study was financed in part by the Coordenação de Aperfeiçoamento de Pessoal de Nível Superior – Brasil (CAPES) – Finance Code 001. André R. Backes gratefully acknowledges the financial support of CNPq (Grant #307100/2021-9). Jarbas Joaci de Mesquita Sá Junior thanks Coordenação de Aperfeiçoamento de Pessoal de Nível Superior (CAPES, Brazil) for the financial support of this work.

REFERENCES

- Backes, A. R., Casanova, D., and Bruno, O. M. (2013). Texture analysis and classification: A complex network-based approach. *Information Sciences*, 219:168 – 180.
- Boser, B. E., Guyon, I. M., and Vapnik, V. N. (1992). A training algorithm for optimal margin classifiers. In *Proceedings of the Fifth Annual Workshop on Computational Learning Theory*, pages 144–152. ACM.
- Calvetti, D., Morigi, S., Reichel, L., and Sgallari, F. (2000). Tikhonov regularization and the l-curve for large discrete ill-posed problems. *Journal of Computational and Applied Mathematics*, 123(1):423–446.
- Chang, C.-C. and Lin, C.-J. (2011). LIBSVM: A library for support vector machines. *ACM Transactions on Intelligent Systems and Technology*, 2:27:1–27:27.
- Cortes, C. and Vapnik, V. (1995). Support-vector networks. *Machine Learning*, 20(3):273–297.
- Cover, T. M. (1965). Geometrical and statistical properties of systems of linear inequalities with applications in pattern recognition. *IEEE Transactions on Electronic Computers*, EC-14(3):326–334.
- Daugman, J. and Downing, C. (1995). Gabor wavelets for statistical pattern recognition. In Arbib, M. A., editor, *The Handbook of Brain Theory and Neural Networks*, pages 414–419. MIT Press, Cambridge, Massachusetts.
- dos Santos, L. F. S., Neves, L. A., Rozendo, G. B., Ribeiro, M. G., do Nascimento, M. Z., and Tosta, T. A. A. (2018). Multidimensional and fuzzy sample entropy (SampEnMF) for quantifying H&E histological images of colorectal cancer. *Computers in Biology and Medicine*, 103:148 – 160.
- Hafiane, A., Palaniappan, K., and Seetharaman, G. (2015). Joint adaptive median binary patterns for texture classification. *Pattern Recognition*, 48(8):2609–2620.
- Huang, G.-B., Zhu, Q.-Y., and Siew, C.-K. (2006). Extreme learning machine: theory and applications. *Neurocomputing*, 70(1):489–501.
- Kather, J. N., Weis, C.-A., Bianconi, F., Melchers, S. M., Schad, L. R., Gaiser, T., Marx, A., and Zollner, F. G. (2016). Multi-class texture analysis in colorectal cancer histology. *Scientific Reports*, 6(27988). doi:10.1038/srep27988.

- Manjunath, B. S. and Ma, W.-Y. (1996). Texture features for browsing and retrieval of image data. *IEEE Trans. Pattern Anal. Mach. Intell.*, 18(8):837–842.
- Moore, E. H. (1920). On the reciprocal of the general algebraic matrix. *Bulletin of the American Mathematical Society*, 26:394–395.
- Nanni, L., Brahnam, S., Ghidoni, S., and Lumini, A. (2019). Bioimage classification with handcrafted and learned features. *IEEE/ACM Transactions on Computational Biology and Bioinformatics*, 16(3):874–885.
- Ojala, T., Pietikäinen, M., and Mäenpää, T. (2002). Multiresolution gray-scale and rotation invariant texture classification with local binary patterns. *IEEE Trans. Pattern Anal. Mach. Intell.*, 24(7):971–987.
- Paladini, E., Vantaggiato, E., Bougourzi, F., Distanti, C., Hadid, A., and Taleb-Ahmed, A. (2021). Two ensemble-CNN approaches for colorectal cancer tissue type classification. *Journal of Imaging*, 7(3).
- Pao, Y.-H., Park, G.-H., and Sobajic, D. J. (1994). Learning and generalization characteristics of the random vector functional-link net. *Neurocomputing*, 6(2):163–180.
- Pao, Y.-H. and Takefuji, Y. (1992). Functional-link net computing: theory, system architecture, and functionalities. *Computer*, 25(5):76–79.
- Penrose, R. (1955). A generalized inverse for matrices. *Mathematical Proceedings of the Cambridge Philosophical Society*, 51(3):406–413.
- Peyret, R., Bouridane, A., Khelifi, F., Tahir, M. A., and Al-Maadeed, S. (2018). Automatic classification of colorectal and prostatic histologic tumor images using multiscale multispectral local binary pattern texture features and stacked generalization. *Neurocomputing*, 275:83 – 93.
- Raczkowski, L., Mozejko, M., Zambonelli, J., and Szczurek, E. (2019). ARA: accurate, reliable and active histopathological image classification framework with Bayesian deep learning. *Scientific Reports*, 9(14347).
- Ribeiro, M. G., Neves, L. A., Nascimento, M. Z., Roberto, G. F., Martins, A. S., and Tosta, T. A. A. (2019). Classification of colorectal cancer based on the association of multidimensional and multiresolution features. *Expert Systems with Applications*, 120:262 – 278.
- Sá Junior, J. J. M. and Backes, A. R. An improved randomized neural network signature for texture classification. *SSRN*.
- Sá Junior, J. J. M. and Backes, A. R. (2016). ELM based signature for texture classification. *Pattern Recognition*, 51:395–401.
- Schmidt, W. F., Kraaijveld, M. A., and Duin, R. P. W. (1992). Feedforward neural networks with random weights. In *Proceedings., 11th IAPR International Conference on Pattern Recognition. Vol.II. Conference B: Pattern Recognition Methodology and Systems*, pages 1–4.
- Siegel, R. L., Miller, K. D., Wagle, N. S., and Jemal, A. (2023). Cancer statistics, 2023. *CA: A Cancer Journal for Clinicians*, 73(1):17–48.
- Tikhonov, A. N. (1963). On the solution of ill-posed problems and the method of regularization. *Dokl. Akad. Nauk SSSR*, 151(3):501–504.
- Wang, C., Shi, J., Zhang, Q., and Ying, S. (2017). Histopathological image classification with bilinear convolutional neural networks. In *2017 39th Annual International Conference of the IEEE Engineering in Medicine and Biology Society (EMBC)*, pages 4050–4053.
- Weszka, J. S., Dyer, C. R., and Rosenfeld, A. (1976). A comparative study of texture measures for terrain classification. *IEEE Trans. Syst., Man, Cyb.*, 6(4):269–285.
- Yoon, H., Lee, J., Oh, J. E., Kim, H. R., Lee, S., Chang, H. J., and Sohn, D. K. (2019). Tumor identification in colorectal histology images using a convolutional neural network. *Journal of Digital Imaging*, 32(1):131–140.